Wind tunnel hardware-in-the-loop experiments about the global response of a 15 MW floating wind turbine

Wind tunnel hardware-in-the-loop experiments about the global response of a 15 MW floating wind turbine

A. Fontanella[1], **A. Facchinetti**[1], **M. Belloli**[1]

[1] Mechanical Engineering Department, Politecnico di Milano, Milano, Via La Masa 1, 20156, Italy.

E-mail: alessandro.fontanella@polimi.it

Abstract. This work describes a new wind tunnel hybrid experiment investigating the aerodynamics and the global response of a 15 MW floating wind turbine. The floater motion is realized with a 6-degrees-of-freedom robotic platform controlled with a hardware-in-the-loop system, in which aerodynamic forces developed by the turbine model are the input of a numerical simulation of the floater dynamics, hydrodynamic excitation, and mooring. It is shown that accuracy of the aerodynamic force feedback from the wind turbine is critical to reproduce the floating wind turbine motion, and measurement of aerodynamic loads is more uncertain in case of pitch motion that movement in the other directions. Free decay tests show that damping of platform surge, pitch, and yaw modes is increased with wind and operating wind turbine compared to the no wind case. The effect of aerodynamic loads on the platform response with stochastic waves is small in the wave frequency range, whereas response of the surge mode is increased with wind.

1. Introduction

Floating offshore wind has large potential, due to the amount of wind resource existing in deep waters (>50m) which is not exploited yet, since traditional bottom-fixed offshore wind is not economically attractive for such locations. A floating wind turbine (FOWT) normally undergoes large motions, that are permitted by the floating foundation, which impact rotor aerodynamics, the action of the turbine-controller and, as a consequence, the system global response. Interactions between these subsystems are not yet fully understood and this lack of knowledge directly affects the reliability of offshore numerical codes and the design of FOWTs in general.

Wind tunnel scale model experiments play a key role in this regard. They are run in controlled conditions and are a reliable way to investigate the physics of the system and to produce data for the validation of numerical codes. Simulation of realistic response of a FOWT requires to emulate at the same time and at small scale all the wind turbine subsystems, which is unpractical to do with physical scale models. One solution is represented by hybrid experiments based on hardware-in-the-loop (HIL), that reproduce only one portion of the FOWT by means of a physical scale model and emulate the rest with a numerical simulation. In particular, hybrid experiments can replicate the functioning of a FOWT including part of the phenomena that are modeled with lower accuracy in offshore codes. In wave basin hybrid testing, the physical portion of the experiment is the platform, mooring, and waves. A survey of wave basin hybrid experiments is found in [1]. More recently, in [2] a 10 MW floating wind turbine is tested with

the hybrid methodology, showing offshore codes do not capture variations in the platform pitch frequency due to static tilt of the platform. In wind tunnel hybrid testing, the physical part of the experiment is the wind turbine and the object of the investigation is the servo-aero-dynamic response with unsteady aerodynamics and the turbine wake. In [3] the surge and pitch response of the DeepCWind and NREL 5 MW is studied for different wind and wave cases, in [4] wind tunnel hybrid tests of two 10 MW FOWTs are carried out.

Despite these efforts, some challenges of hybrid testing are yet to be solved. This paper contributes to the advancement of wind tunnel hybrid testing technology presenting results of the HIL experiment of a 15 MW FOWT, recently performed in the atmospheric boundary layer wind tunnel of Politecnico di Milano. In particular, it advances the present state of knowledge by investigating the effect of HIL control system on the wind turbine global response and on the emulation of aerodynamic loads. Free decay and irregular wave tests are carried out to assess the effect of rotor loads on the FOWT global response. In particular, we analyze platform motion in surge and pitch directions, which, according to previous studies [5], are the most affected by aerodynamic excitation.

2. Description of the experiment

The object of the experimental testing is the FOWT formed by the IEA 15 MW [6] and the Activefloat semisubmersible platform [7]. In the hybrid approach, the aerodynamic loading of the rotor is reproduced with a physical scale model of the wind turbine, and the rest of the FOWT with a simulation model. These two subsystems are joined by the HIL control system. The wind turbine model is used to reproduce aerodynamic loads only, and not inertia forces and weight, thus Froude scaling is not required [8].

The scaling adopted in the experiment maximizes Reynolds number with a wind turbine scale model of the maximum size compatible with the wind tunnel test section dimensions. The scale factor for wind speed is chosen based on frequency requirements (e.g., rotor speed, flexible response of the turbine components). The geometry scale factor is set to 1:100, and the scale factor for velocity is 1:4. Scale factors for all other quantities are obtained from the geometry and velocity scale factors by means of dimensional analysis. Experiments are run with an empty-inlet configuration, wind speed is uniform across the wind tunnel section and turbulence intensity is about 2%. The test setup is shown in Fig. 1 together with the coordinate systems (CSs) that are used in the experiment.

2.1. Physical subsystem: the wind turbine scale model

The physical part of the experiment is the wind turbine rotor and wind. Because of scaling, the Reynolds number for the turbine scale model is lower than 100k. The rotor of the wind turbine model is designed based on the methodology introduced in [9] for a 1:75 scale model of the DTU 10 MW, to match with good accuracy the aerodynamic response of the IEA 15 MW. The low-Reynolds SD7032 airfoil is used along the blade, whose chord and twist are defined to preserve part of the characteristics of the IEA 15 MW rotor: the design TSR, the chord distribution, the axial blade loading, the variation of axial force due to a variation of TSR or blade pitch. Blades are constructed to be as rigid as possible. The wind turbine has the ability to apply active generator and blade pitch control, however the tests presented here only consider steady conditions with fixed rotor speed and blade pitch angle. The tower is an aluminum tube of 75 mm diameter, and the first flexible mode of the turbine is at 9.5 Hz.

2.2. Numerical subsystem: the hydrodynamic and platform model

The floating structure with mooring and waves forms the numerical subsystem, reproduced in the experiment by means of a simulation model. The model is based on the time-domain

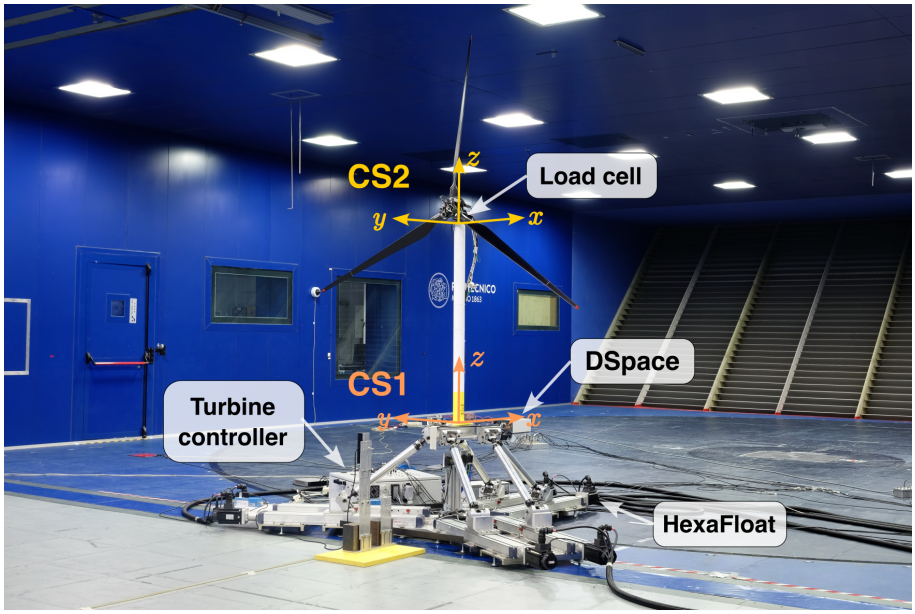

Figure 1. Test setup inside the wind tunnel and coordinate systems: platform (CS1) and nacelle (CS2).

equation of motion of the support platform, which is widely used in offshore wind turbine tools [10]:

$$(\boldsymbol{M} + \boldsymbol{A}_\infty)\ddot{\boldsymbol{q}}_\mathrm{s} = \boldsymbol{F}_\mathrm{hs} + \boldsymbol{F}_\mathrm{moor} + \boldsymbol{F}_\mathrm{rad} + \boldsymbol{F}_\mathrm{wave} + \boldsymbol{F}_\mathrm{visc} + \boldsymbol{F}_\mathrm{wt,n}\,, \tag{1}$$

where $\boldsymbol{M}$ is the mass matrix of the FOWT (formed by platform, tower, rotor-nacelle that are modeled as rigid bodies, see [11]), $\boldsymbol{A}_\infty$ the infinite-frequency added mass, $\ddot{\boldsymbol{q}}_\mathrm{s}$ the second time derivative of the platform rigid-body motions in CS1: surge, sway, heave, roll, pitch, yaw. The external loads are: hydrostatic forces $\boldsymbol{F}_\mathrm{hs}$, mooring forces $\boldsymbol{F}_\mathrm{moor}$, radiation forces $\boldsymbol{F}_\mathrm{rad}$, wave excitation forces $\boldsymbol{F}_\mathrm{wave}$, the non-linear viscous drag loads $\boldsymbol{F}_\mathrm{visc}$, and wind turbine aerodynamic forces $\boldsymbol{F}_\mathrm{wt,n}$. This last term couples the physical subsystem to the numerical subsystem and it is obtained from measurements. The remaining forces are obtained numerically. $\boldsymbol{F}_\mathrm{hs}$, $\boldsymbol{F}_\mathrm{rad}$, and $\boldsymbol{F}_\mathrm{wave}$ are modeled with potential flow, with pre-computed frequency-dependent hydrodynamic coefficients obtained from WAMIT. $\boldsymbol{F}_\mathrm{wave}$ include first- and second-order (difference frequency) hydrodynamic loads. Stochastic waves are generated analytically using first-order wave theory. Equation 1 is integrated in a time-marching simulation to compute the platform motion $\boldsymbol{q}_\mathrm{s}$. The numerical model is run at model scale to respect the time scale of the experiment.

3. Hardware-in-the-loop control system

In the hybrid experiment the physical link between the hydro-structural response of the FOWT and the servo-aerodynamic response of the rotor is obtained with the HIL control system that couples the numerical and physical subsystems. The scheme of the HIL control system is shown in Fig. 2. It consists of measurement of forces at the tower-nacelle interface, real-time processing of these measurements to extract the rotor aerodynamic forces, and a motion system that moves the wind turbine tower base according to the output of the numerical model.

3.1. Measurement system: force feedback

Wind turbine forces $\boldsymbol{F}_\mathrm{wt}$ are obtained from the 6-components interface forces measured at the tower-nacelle connection in CS2, that are expressed in CS1, to be in the same coordinate system

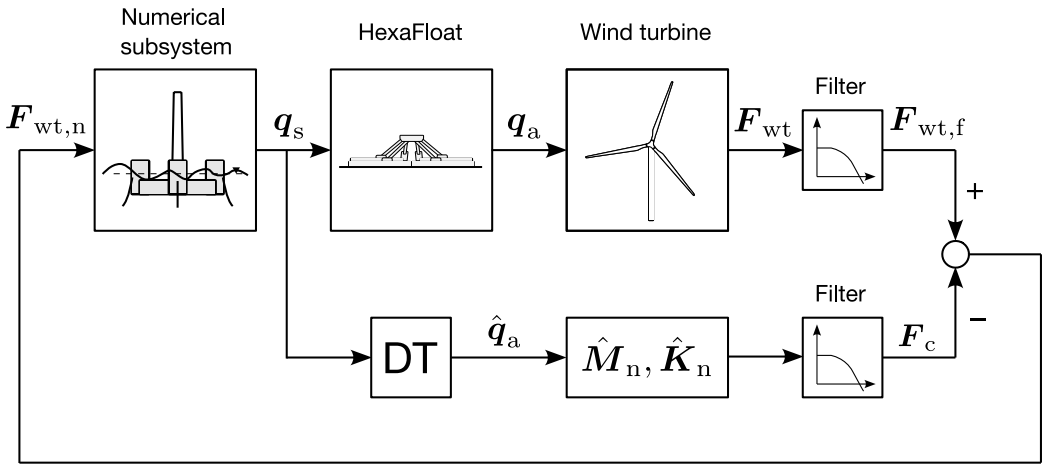

Figure 2. Scheme of the HIL control system.

of Eq. 1. $\boldsymbol{F}_{\mathrm{wt,f}}$ is obtained from $\boldsymbol{F}_{\mathrm{wt}}$ which is filtered to remove contributions due to the turbine flexible response. The filter is a second-order Butterworth filter with cutoff frequency 3 Hz, in series with a second-order notch filter with frequency 9.5 Hz (i.e., the first tower fore-aft bending mode). The force feedback to the numerical subsystem is the rotor aerodynamic loads, that has to be obtained depriving $\boldsymbol{F}_{\mathrm{wt,f}}$ of mechanical loads $\boldsymbol{F}_{\mathrm{c}}$:

$$\boldsymbol{F}_{\mathrm{wt,n}} = \boldsymbol{F}_{\mathrm{wt,f}} - \boldsymbol{F}_{\mathrm{c}} \,. \tag{2}$$

In the current implementation of the HIL control system, $\boldsymbol{F}_{\mathrm{c}}$ accounts for the inertia and weight of the rotor-nacelle assembly (RNA) originating with rigid-body platform motion. With linear formulation:

$$\boldsymbol{F}_{\mathrm{c}}^{*} = \hat{\boldsymbol{M}}_{\mathrm{n}} \ddot{\hat{\boldsymbol{q}}}_{\mathrm{a}} + \hat{\boldsymbol{K}}_{\mathrm{n}} \hat{\boldsymbol{q}}_{\mathrm{a}} \,, \tag{3}$$

where $\hat{\boldsymbol{q}}_{\mathrm{a}}$ is the estimated actual platform motion. Mechanical loads are assumed proportional to the acceleration of the wind turbine with matrix $\hat{\boldsymbol{M}}_{\mathrm{n}}$, and to its position with matrix $\hat{\boldsymbol{K}}_{\mathrm{n}}$. These matrices are obtained combining system identification and first-principle modeling based on multi-body system dynamics theory. The force $\boldsymbol{F}_{\mathrm{c}}^{*}$ is filtered with the same filter applied to the wind turbine force to have $\boldsymbol{F}_{\mathrm{c}}$.

3.2. Motion system

Platform motion computed from real-time integration of Eq. 1 is recreated in the physical domain of the experiment with a 6-DOFs robotic platform mounted under the base of the turbine tower. The robot, which design is covered in [12], is of parallel kinematic type. Calculation of the force-feedback with Eq. 3 requires the turbine actual position $\boldsymbol{q}_{\mathrm{a}}$. This is not directly available from the robot, but it is estimated from the position setpoint $\boldsymbol{q}_{\mathrm{s}}$ and the dynamic model of the robot ($\boldsymbol{q}_{\mathrm{s}} \rightarrow \hat{\boldsymbol{q}}_{\mathrm{a}}$). In this work, the robot is modeled as a pure-delay system with a delay of 0.03 s.

3.3. Verification of the HIL control system

The coupling between numerical and physical subsystems realized with HIL control must be transparent, i.e. it must not affect the physics of the FOWT. The transparency is influenced by sensor accuracy, actuation speed and accuracy, and the representation of the rotor mechanical forces in the $\boldsymbol{F}_{\mathrm{c}}$ model.

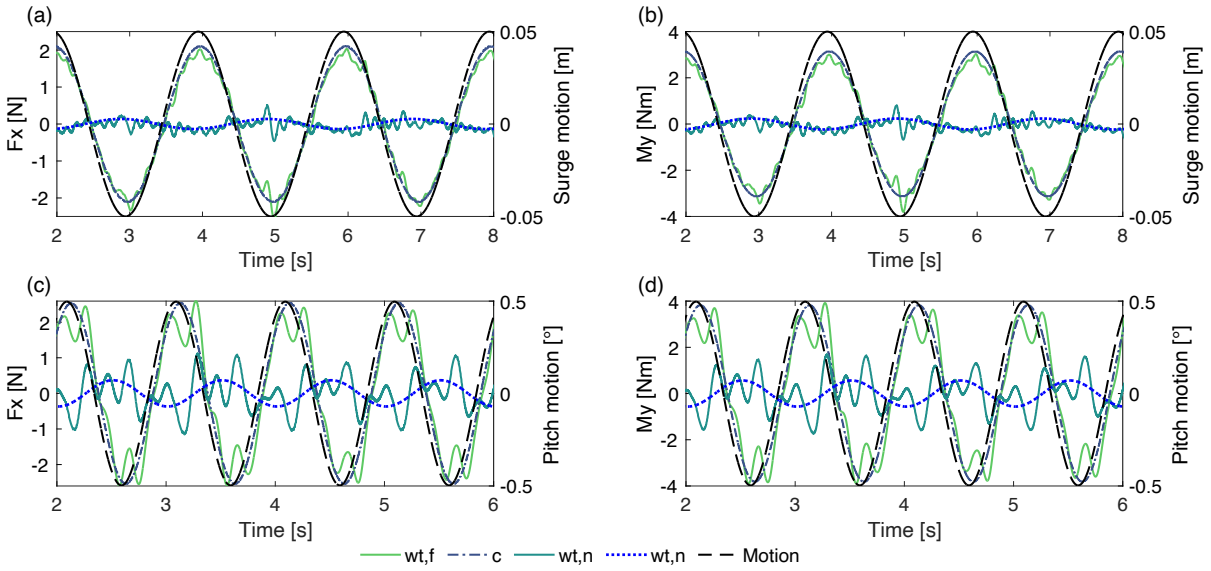

Figure 3. Time series of wind turbine forces with imposed sinusoidal motion in: **(a,b)** surge, and **(c,d)** pitch directions. "wt,f" is the filtered force measurement, "c" are the mechanical loads of the physical rotor-nacelle assembly, "wt,n" is their difference which represents the force feedback to the numerical subsystem.

Transparency is verified with imposed motion tests in still air with no force feedback, i.e. $\boldsymbol{F}_{\mathrm{wt,n}} = 0$ in Eq. 1. Harmonic motion of several combinations of frequency f and amplitude A is imposed along one platform direction at a time. Since there is no wind, aerodynamic forces are negligible, the wind turbine loads are mainly due to nacelle weight and inertia, and it is expected that $\boldsymbol{F}_{\mathrm{wt,f}} - \boldsymbol{F}_{\mathrm{c}} \approx 0$. This is verified in Fig. 3 with surge motion ($f = 0.5$ Hz, $A = 0.05$ m) and pitch motion ($f = 1.0$ Hz, $A = 0.5°$). In case of surge, $F_{x,\mathrm{wt,f}}$ and $M_{y,\mathrm{wt,f}}$ are due to nacelle inertia and are in phase with motion. In this case $\boldsymbol{F}_{\mathrm{c}}$ slightly overestimates $\boldsymbol{F}_{\mathrm{wt,f}}$: the net forces $\boldsymbol{F}_{\mathrm{wt,n}}$ have a small component at the frequency of motion (1-harmonic) with superposed high-frequency content that is not filtered and is not captured by $\boldsymbol{F}_{\mathrm{c}}$. The 1-harmonic has a phase difference of about 180° with respect to motion. When this force is the feedback to the numerical system, it is expected to slightly decrease the inertia of the FOWT. In case of surge motion, $\boldsymbol{F}_{\mathrm{c}}$ requires an estimate of the RNA mass; this is obtained weighing the rotor-nacelle components and is accurate. In case of pitch motion, $F_{x,\mathrm{wt,f}}$ and $M_{y,\mathrm{wt,f}}$ are due to the nacelle inertia and weight and have a slight phase shift with respect to motion. The difference between $\boldsymbol{F}_{\mathrm{wt,f}}$ and $\boldsymbol{F}_{\mathrm{c}}$ is larger than in case of surge; the net forces $\boldsymbol{F}_{\mathrm{wt,n}}$ are not negligible and have a component at the frequency of motion plus some oscillations at 3 Hz. The 1-harmonic has a phase difference of about 160° with respect to motion: when this force is the feedback to the numerical system, it affects inertia and damping of the FOWT. In case of pitch motion, $\boldsymbol{F}_{\mathrm{c}}$ requires an estimate of the RNA moment of inertia which is difficult to get. Moreover, hub linear acceleration with surge is lower than with pitch, thus inertial loads to be removed with surge motion are lower than with pitch.

4. Response of the floating wind turbine

Load cases are free-decay tests for the surge, pitch and yaw DOFs, and irregular wave tests with JONSWAP or white-noise waves. Tests are run in no wind and with two wind turbine operating conditions summarized in Table 1. No wind load cases are repeated with two configurations of

the HIL control system: in open-loop, when the force feedback from the turbine $\boldsymbol{F}_{\mathrm{wt,n}}$ is set to zero; and with enabled force feedback. The open-loop configuration is equivalent to imposed motion, where motion is computed in real-time considering there are no aerodynamic loads from the wind turbine. All results in this section are reported at full-scale.

Table 1. Wind turbine operating conditions considered in the experiment (β is collective pitch).

Condition	Wind speed [m/s]	Rotor speed [RPM]	β [°]
Below rated	8.5	6.47	1.2
Above rated	17.5	7.56	14.1

4.1. Free decay

In free decay tests an initial condition is applied alternatively to the surge, pitch, and yaw DOFs. The response of the DOF subjected to the initial condition is examined to estimate damping and frequency of the FOWT rigid-body modes. Free motion is reported in Fig. 4 for the open-loop and the HIL configurations of the system, with different wind conditions. The linear properties of the surge, pitch, and yaw modes, reported in Table 2, are obtained from the time series of Fig. 4 by means of the logarithmic decrement method (considering the first 5 consecutive peaks); in the pitch case, the response in some wind conditions has no cyclic oscillations, thus the linear properties are obtained computing the time-domain specifications of the equivalent second-order system.

For surge, the no wind (HIL) response is very close to the one with open-loop, as expected. In this condition of motion, the HIL control system is transparent and does not modify the FOWT response. This is in agreement with verification of the HIL control system, where it is seen that mechanical loads are removed effectively in case of surge motion. With wind, the surge mode frequency does not change and damping is increased. For yaw, the HIL-no wind response is similar to the open-loop case. Damping is higher in no wind compared to open-loop, but it is still lower than 1%. The effect of wind is to increase damping of the yaw mode, and the increment is larger than for the surge mode. For pitch motion, the response with open-loop is more damped and of higher frequency than response with HIL-no wind. In this case, the effect of the HIL control system on the FOWT response is not negligible. Also for pitch, wind increases damping, which is a lot higher in above rated compared to below rated. The lower accuracy of HIL control in the pitch case is due to the difference between $\boldsymbol{F}_{\mathrm{c}}$ and $\boldsymbol{F}_{\mathrm{wt,f}}$ that is commented in Sec. 3.3. The non-zero force feedback has a contribution due to RNA inertia and weight that is only partially removed by the HIL control system, and this force contribution changes the response of the FOWT when the force feedback is activated. In case of pitch, the force feedback has residual high-frequency contributions due to nacelle weight and inertia, visible in Fig. 3, which are responsible of the low-amplitude oscillations in the last part of the decay.

4.2. Irregular waves

Among all wave conditions considered in the experiment, here we examine the case of white-noise waves with zero-degree heading, aligned with the wind direction. The wave spectrum has amplitude $H_s^{2/8}$ for frequencies in the range $[1/26, 1/6]$ Hz and zero outside, $H_s = 1.9$ m. First- and second-order wave forces are modeled.

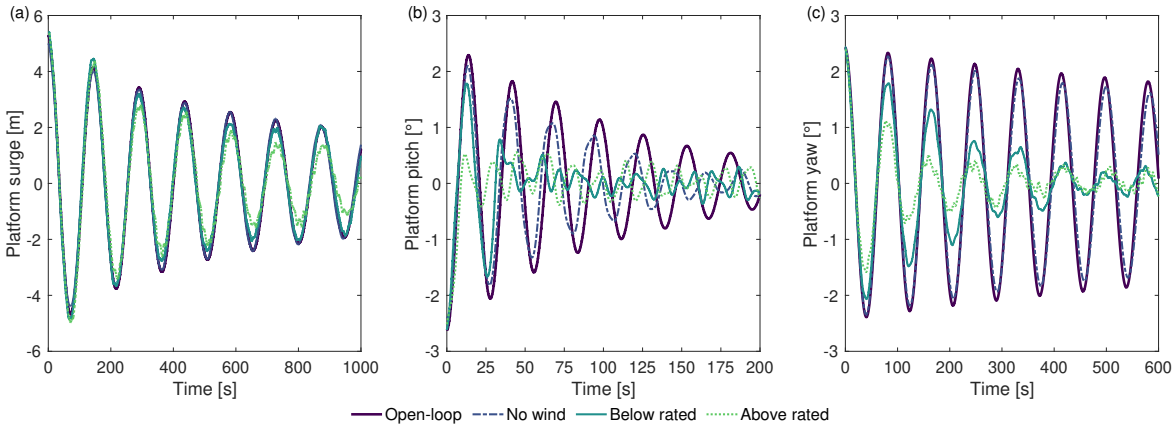

Figure 4. Platform motion in free-decay tests without force feedback (Open-loop), with force feedback and different wind conditions. **(a)** surge motion with surge decay, **(b)** pitch motion with pitch decay, **(c)** yaw motion with yaw decay.

Table 2. Frequency (f) and damping ratio (ξ) for platform surge, pitch and yaw modes from free decay tests.

Configuration	Surge		Pitch		Yaw	
	f [Hz]	ξ [-]	f [Hz]	ξ [-]	f [Hz]	ξ [-]
Open-loop	0.0069	0.0208	0.0344	0.0306	0.0120	0.0053
No wind	0.0069	0.0181	0.0364	0.0437	0.0199	0.0077
Below rated	0.0069	0.0256	0.0407	0.0649	0.0120	0.0417
Above rated	0.0068	0.0330	0.0503	0.4067	0.0133	0.0486

Platform response to waves is studied computing the transfer function between wave elevation and platform motion, i.e. the response amplitude operator (RAO). The information provided by RAO is complemented with the magnitude-squared coherence function:

$$\gamma^2(f) = \frac{|P_{\eta x}(f)|^2}{P_{\eta\eta}(f)P_{xx}(f)}\,, \tag{4}$$

which is a function of the power spectral densities of the wave $P_{\eta\eta}(f)$, of the platform motion $P_{xx}(f)$, and of their cross power spectral density $P_{\eta x}(f)$. γ^2 is a function of frequency with values between 0 and 1, indicating how well platform motion corresponds to wave at each frequency. RAO and γ^2 are estimated using the Welch's overlapped averaged periodogram method.

The RAOs and coherence for platform surge and pitch for different wind turbine operating conditions and HIL configurations are reported in Fig. 5. For surge, RAOs are overlapped in the wave frequency range. At these frequencies, γ^2 for the HIL-no wind and open-loop cases is close to 1, meaning that platform motion is highly correlated to wave. Amplitude of surge motion at the surge frequency is higher in the HIL-no wind case compared to open-loop. This is attributed to residual mechanical loads that are not completely removed from $\boldsymbol{F}_{\mathrm{wt,n}}$, which effect is to decrease damping of the surge mode, as seen in free-decay tests (see Table 2). With wind, the response in the wave frequency range is unchanged, but it is increased in the low frequency range. Here, $\gamma^2 \approx 0$: the platform response is due to second-order wave forces and wind turbine forces. For pitch, the RAOs in the wave-frequency range are not overlapped. $\gamma^2 \approx 1$ for the open-loop system, but it is lower for cases with HIL; in particular it is lower than 0.5 up to 0.1

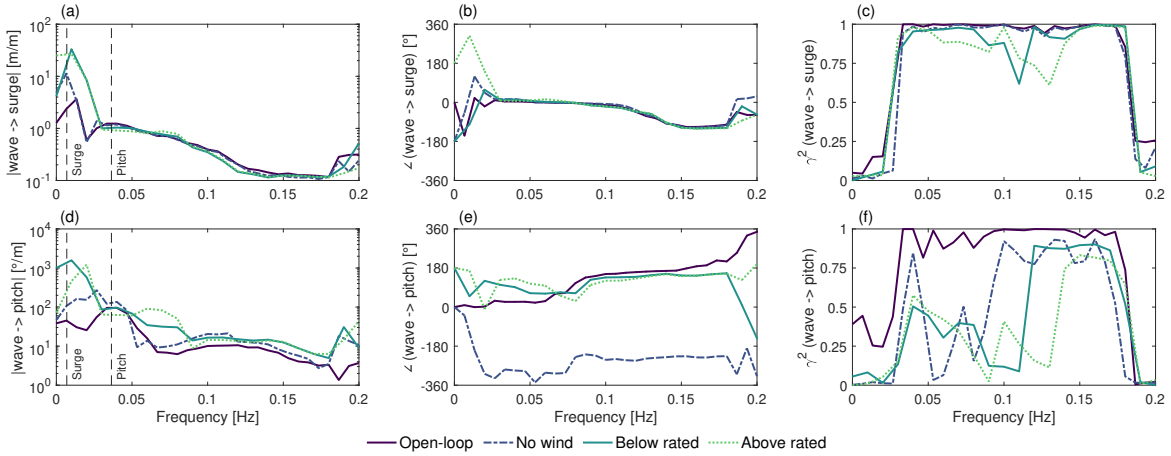

Figure 5. Response amplitude operators with white-noise irregular waves for the system without force feedback (Open-loop), with force feedback and different wind conditions: **(a,b,c)** surge, **(d,e,f)** pitch. Vertical dashed lines mark the frequency of the platform surge and pitch modes.

Hz. When the HIL force feedback is active, the coherence between platform response and wave is lower, because part of the mechanical loads of the physical RNA is not removed from $\boldsymbol{F}_{\mathrm{wt,n}}$ and represents a non negligible fraction of the total excitation for the FOWT. In the low-frequency range, RAO amplitude at the pitch mode frequency is about constant for all conditions. It changes significantly at the surge mode frequency, where it is minimum in the open-loop case and increases when the force feedback is activated. As for surge, the response amplitude with wind is higher than with no wind.

Wave loads (first- and second-order) and the wind turbine forces are examined in the HIL-no wind case to better understand the influence of the HIL control system on platform response to waves. In particular, we look at F_{x} and M_{y} that are the main excitation loads for surge and pitch motion respectively. Figure 6 shows the time series and spectra of these forces with the same white-noise irregular waves of Fig. 5. For F_{x}, the wave force is dominant over the wind turbine force across the entire frequency range of interest. $F_{\mathrm{x,c}} \approx F_{\mathrm{x,wt,f}}$ up to 0.75 Hz. Above this frequency, the difference is higher due to the flexibility of the wind turbine components, which is not modeled in $\boldsymbol{F}_{\mathrm{c}}$ (see Eq. 3). At any frequency, the force feedback $F_{\mathrm{x,n}}$ is lower in magnitude than wave force: at 0.05 Hz, $F_{\mathrm{x,n}} \approx 34 F_{\mathrm{x,wave}}$. For M_{y} the RNA mechanical loads are correctly captured in $M_{\mathrm{y,c}}$ up to 0.75 Hz, where $M_{\mathrm{y,c}} \approx M_{\mathrm{y,wt,f}}$. However, in this case, the wave force is similar in magnitude to wind turbine forces across the entire frequency range of interest. At 0.05 Hz $M_{\mathrm{y,n}} \approx 2.7 M_{\mathrm{y,wave}}$. At this frequency, excitation due to the residual mechanical loads of the physical RNA and loads due to wave are of equal importance, and this explains the lower correlation between wave and platform pitch motion shown by γ^2 in Fig. 5.

5. Conclusions

Hybrid wind tunnel experiments are a recognized tool for the validation of offshore codes and to advance knowledge about the aerodynamics of FOWTs. Despite recent efforts, it is not clear which is the best architecture for the HIL system. This work has investigated the effect of HIL control on the global response of a FOWT with a new experiment about the Activefloat 15 MW floating wind turbine.

In the present case, the feedback signal connecting the physical portion of the experiment to the numerical one is the rotor aerodynamic loading. Direct measurement of aerodynamic

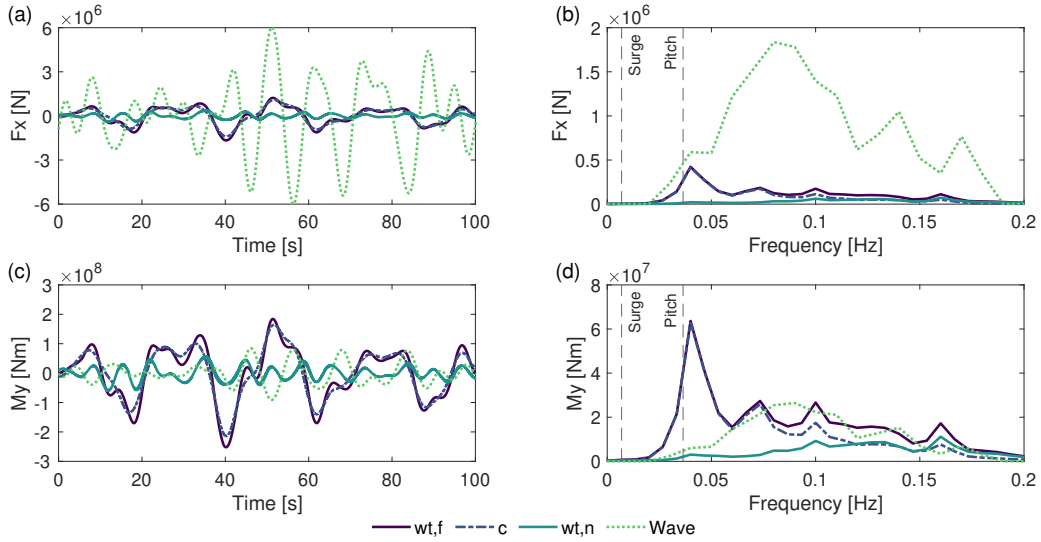

Figure 6. Time series and spectra of wind turbine and wave forces with white-noise irregular waves and no wind: **(a,b)** F_x, **(c,d)** M_y. "wt,f" is the filtered force measurement, "c" are the mechanical loads of the physical rotor-nacelle assembly, "wt,n" is their difference which represents the force feedback to the numerical subsystem, "wave" is the wave excitation force. Vertical dashed lines mark the frequency of the platform surge and pitch modes.

loads is not available, and they are estimated from tower-top interface forces. It is shown that estimation errors are present, and are due to identification of the RNA mass properties. In general, aerodynamic loads estimation is found to be less accurate in case of pitch motion; wave forcing and RNA inertia force in the pitch direction are of comparable magnitude. For these reasons, pitch motion is reproduced with lower accuracy than motion in other directions, and it is more difficult to quantify the influence of aerodynamics loads on the platform pitch response than on surge and yaw. The effect of wind on damping and frequency of the platform surge, pitch, and yaw modes is studied in free decay tests. Damping is higher when the turbine is operating compared to the no wind case. Tests with white-noise waves show that the platform surge and pitch response in the wave frequency range is not affected by aerodynamic loads, but in the low-frequency range the response amplitude is higher with operational turbine.

In the light of these findings, future work about HIL technology for wind tunnel testing of FOWTs should target the coupling between wind turbine scale model and numerical subsystem. One research path is to improve the aerodynamic loads estimation, for example using a different sensor that is not affected as much by mechanical forces of the RNA, or improving the method used to remove them, possibly based on system identification or data-driven modeling. Another research path is to use the total RNA loads, inclusive of weight and inertia, as feedback. In this way, estimation of aerodynamic loads is not required, but Froude scaling becomes mandatory, losing part of the advantages of hybrid HIL testing. In parallel, a better understanding of the effect of aerodynamic loading on the global response of FOWTs can be gained comparing experimental data from hybrid experiments and simulations with fully-coupled offshore simulation codes.

6. Acknowledgements

This research has been supported by the Horizon 2020 (COREWIND (grant no. 815083)).

References

[1] S. Gueydon, R. Lindeboom, W. van Kampen, and E.-J. de Ridder. Comparison of Two Wind Turbine Loading Emulation Techniques Based on Tests of a TLP-FOWT in Combined Wind, Waves and Current. ASME 2018 1st International Offshore Wind Technical Conference, 11 2018. V001T01A012.

[2] F. Vittori, J. Azcona, I. Eguinoa, O. Pires, A. Rodríguez, Á. Morató, C. Garrido, and C. Desmond. Model tests of a 10 mw semi-submersible floating wind turbine under waves and wind using hybrid method to integrate the rotor thrust and moments. *Wind Energy Science*, 7(5):2149–2161, 2022.

[3] I. Bayati, A. Facchinetti, A. Fontanella, F. Taruffi, and M. Belloli. Analysis of FOWT dynamics in 2-DOF hybrid HIL wind tunnel experiments. *Ocean Engineering*, 195, 2020.

[4] M. Belloli, I. Bayati, A. Facchinetti, A. Fontanella, H. Giberti, F. La Mura, F. Taruffi, and A. Zasso. A hybrid methodology for wind tunnel testing of floating offshore wind turbines. *Ocean Engineering*, 210, 2020.

[5] A. Fontanella, A. Facchinetti, S. Di Carlo, and M. Belloli. Wind tunnel investigation of the aerodynamic response of two 15 mw floating wind turbines. *Wind Energy Science*, 7(4):1711–1729, 2022.

[6] E. Gaertner, L. Rinker, J. and. Sethuraman, F. Zahle, B. Anderson, G. Barter, N. Abbas, F. Meng, P. Bortolotti, W. Skrzypinski, G. Scott, R. Feil, H. Bredmose, K. Dykes, M. Shields, C. Allen, and A. Viselli. Definition of the IEA 15-Megawatt Offshore Reference Wind Turbine, Tech. rep., National Renewable Energy Laboratory. 2020. Available at https://www.nrel.gov/docs/fy20osti/75698.pdf.

[7] M. Y. Mahfouz, C. Molins, P. Trubat, S. Hernández, F. Vigara, A. Pegalajar-Jurado, H. Bredmose, and M. Salari. Response of the international energy agency (iea) wind 15 mw windcrete and activefloat floating wind turbines to wind and second-order waves. *Wind Energy Science*, 6(3), 2021.

[8] I. Bayati, A. Facchinetti, A. Fontanella, H. Giberti, and M. Belloli. A wind tunnel/hil setup for integrated tests of floating offshore wind turbines. *Journal of Physics: Conference Series*, 1037(5):052025, jun 2018.

[9] I. Bayati, M. Belloli, L. Bernini, and A. Zasso. Aerodynamic design methodology for wind tunnel tests of wind turbine rotors. *Journal of Wind Engineering and Industrial Aerodynamics*, 167:217 – 227, 2017.

[10] J. Jonkman. Dynamics modeling and loads analysis of an offshore floating wind turbine, tech. rep., national renewable energy laboratory. 01 2007. Available at https://www.nrel.gov/docs/fy08osti/41958.pdf.

[11] S. Ambrosini, I. Bayati, A. Facchinetti, and M. Belloli. Methodological and Technical Aspects of a Two-Degrees-of-Freedom Hardware-In-the-Loop Setup for Wind Tunnel Tests of Floating Systems. *Journal of Dynamic Systems, Measurement, and Control*, 142(6), 03 2020. 061002.

[12] H. Giberti, F. La Mura, G. Resmini, and M. Parmeggiani. Fully mechatronical design of an hil system for floating devices. *Robotics*, 7(3), 2018.